Dynamics of Nitrogen Scattering off N-covered Ag(111)

M. Blanco-Rey,[†] L. Martin-Gondre,[†,‡] R. Díez Muiño,[†,‡] M. Alducin,[†,‡] and J.I. Juaristi[†,‡,¶]

† Donostia International Physics Center, Paseo Manuel de Lardizabal 4, 20018 Donostia-San Sebastián, Spain

‡ Centro de Física de Materiales, Centro Mixto CSIC-UPV/EHU, Paseo Manuel de Lardizabal 5, 20018 Donostia-San Sebastián, Spain

¶ Departamento de Física de Materiales, Facultad de Químicas UPV/EHU, Apartado 1072, 20018 Donostia-San Sebastián, Spain

J. Phys. Chem. C, 2012, 116, pp 21903-21912

http://dx.doi.org/10.1021/jp3074514

Dynamics of Nitrogen Scattering off N-covered Ag(111)

M. Blanco-Rey,[*,†] L. Martin-Gondre,[†,‡] R. Díez Muiño,[†,‡] M. Alducin,[†,‡] and J.I. Juaristi[†,‡,¶]

Donostia International Physics Center, Paseo Manuel de Lardizábal 4, 20018 Donostia-San Sebastián, Spain, Centro de Física de Materiales, Centro Mixto CSIC-UPV/EHU, Paseo Manuel de Lardizábal 5, 20018 Donostia-San Sebastián, Spain, and Departamento de Física de Materiales, Facultad de Químicas UPV/EHU, Apartado 1072, 20018 Donostia-San Sebastián, Spain

E-mail: maria_blancorey@ehu.es

Abstract

We analyze the reflection and adsorption dynamics of N atoms on a (1×1) N-covered Ag(111) surface, using an ab-initio three-dimensional potential energy surface (3D PES) and classical molecular dynamics (MD) in the frozen and vibrating surface regimes. Our calculations reveal strong changes in the PES upon atomic N adsorption, which becomes much more corrugated than that of the clean Ag(111) surface. This apparently contradicts a key experimental finding made for atoms with incident average energy $\langle E_i \rangle = 4.3\,\text{eV}$, namely that the N reflection dynamics on Ag(111) at N saturation coverage are quantitatively similar to those

[*]To whom correspondence should be addressed

[†] Donostia International Physics Center, Paseo Manuel de Lardizábal 4, 20018 Donostia-San Sebastián, Spain

[‡] Centro de Física de Materiales, Centro Mixto CSIC-UPV/EHU, Paseo Manuel de Lardizábal 5, 20018 Donostia-San Sebastián, Spain

[¶] Departamento de Física de Materiales, Facultad de Químicas UPV/EHU, Apartado 1072, 20018 Donostia-San Sebastián, Spain

of clean Ag(111). In good agreement with the experiments, we find that the stronger PES corrugation of the N-covered Ag(111) surface does not affect the angular distribution of the scattered N atoms with that $\langle E_i \rangle$ value. However, discrepancies are found in the final-to-initial average energy ratios, $\langle E_f \rangle / \langle E_i \rangle$, at grazing outgoing angles. Upon examination of the adsorption trajectories, it can be inferred that gas N is likely to react with adsorbed N. MD shows that this "pick-up" mechanism is particularly effective for slow atoms and could be behind the experimental $\langle E_f \rangle / \langle E_i \rangle$ values.

Keywords: Gas/surface dynamics; Adsorption; Non-adiabatic effects; Inelastic scattering; Density functional theory; Eley-Rideal reactions

Introduction

Molecular and atomic beam scattering is an excellent tool to explore the characteristics of the interaction between molecular and atomic particles with metal surfaces. Properties of the reflected particles after their interaction with the surface, such as the scattering angle distributions, as well as the translational energy and rovibrational state distributions, are closely related to the nature of the interaction potential energy hypersurface. The potential energy landscape is particularly rich and involved for the case of reactive species. In the last years, with the development of ab-initio calculations based on density functional theory (DFT), a great accuracy in the characterization of these systems and, correspondingly, in the gas-surface dynamics simulations has finally been achieved.[1–11]

The interaction of hyperthermal Nitrogen atoms with Ag(111) constitutes a representative case of such reactive systems that has recently attracted attention.[12,13] Though the N_2 molecule is very unreactive towards the Ag(111) surface,[14–16] when the molecular bond is broken, the resulting N atoms interact strongly with this surface. As a result, the corresponding potential energy surface (PES) for an N atom interacting with a clean Ag(111) surface is very corrugated.[17] This is reflected in the measured broad angular distributions of reflected N atoms upon scattering with this

surface.[12]

When an adsorbate is already present on a surface, the PES, and therefore the gas-surface dynamics, are expected to be very different from those of the clean surface. For instance, it has been observed that pre-adsorbed CO on Ru(0001) acts as a pasivator for the dissociation of impinging D_2 molecules.[18] DFT has proved to be a reliable tool to understand another relevant case, namely the modification of H_2 reactivity on Pd(100) by adsorbed species. For example, the poisoning effect of S adsorbates has been proved to occur via an enhancement of the PES corrugation, resulting in new barriers for H-H bond breaking.[19–21] The PES details also explain, beyond a mere site blocking picture, the reduction in the dissociative adsorption of H_2 on a H-covered Pd(100) surface.[8,22,23] However, recent experiments carried out on the N-covered Ag(111) surface showed, for hyperthermal N atoms scattered off this surface, that the angular distributions and the angle resolved energy distributions were strikingly similar to those obtained in the bare Ag(111) surface.[13] Motivated by these unexpected results we have calculated the PES for a N atom interacting with an N-covered Ag(111) surface using first principles calculations, and performed classical molecular dynamics (MD) simulations to understand these experimental observations. Since the experiments were carried out at saturation coverage, we choose a model surface where all the fcc-like hollow sites of the lattice are occupied by an adsorbed N atom, i.e. the lattice has (1×1) periodicity. However, we note that the actual coverage under experimental conditions, which is in principle an unknown magnitude, might be slightly lower. This seems to be a plausible scenario when additional experimental results are considered that the incident N atoms might recombine with adsorbed N, leading to the desorption of N_2 molecules .[13]

The beam experiments that report recombinative abstraction of adsorbed species using neutral projectiles of energies in the range ≤ 10 eV have traditionally involved hydrogen or deuterium as projectiles or adsorbed species.[24–30] Other examples of gas-surface reactions have been reported that involved atomic O projectiles and molecular adsorbate targets on the surface, such as CO[31] and O_2.[32] For this reason, the possibility that surface N atoms are abstracted by N projectiles in the form of N_2 constitutes an encouraging outcome of these experiments. An additional bonus of

our analysis is the possibility to explore whether this process is conceivable for this system and, if this were the case, to gain some information on its likelihood and main features.

The paper is organized as follows: a description of the theoretical procedure is made first that accounts for the DFT calculation details, the PES interpolation scheme and the settings in the MD simulations. The results section begins with an analysis of the interpolated PES topography, followed by the scattering distributions obtained from the MD simulations. Afterwards, a thorough analysis of reflected and adsorbed atom trajectories is made as a function of the incident energy.

Theory

The scattering of gas N atoms on the N-covered Ag(111) surface is simulated by performing classical molecular dynamics (MD) calculations using an accurate three-dimensional potential energy surface (3D PES) that is calculated from first-principles. Compared with the *on the fly ab-initio* molecular dynamics (AIMD) that in the last years is becoming computationally more affordable,[8,22,33] the methodology followed here is in principle more tedious because it requires various steps: (i) calculation of a sufficiently dense grid of *ab-initio* potential energies, (ii) accurate interpolation of the *ab initio* data to assure small energy errors at each point of the incident N trajectory, and (iii) integration of the classical equations of motion. However, it also offers a series of advantages over the AIMD once the PES is constructed. On the one hand, the results of the dynamics calculations can be easily combined with the detailed information of the PES properties to single out the factors ruling the scattering process. On the other hand, it allows a large number of trajectory calculations at almost none additional computational cost. This is a crucial point in our case because the experimental effusive beam of Ref.[13] has required an extensive amount of calculations in order to assure a reliable statistical description of the incidence conditions and of the final outgoing angle and energy distributions measured in the experiments (*vide infra*).

The details of the theoretical calculations performed at each step follow.

DFT calculation details

Spin-polarized DFT calculations are carried out with the VASP code[34] using an energy cutoff of 348 eV in the plane-wave basis set and ultra-soft pseudopotentials[35] to describe the core electrons. The exchange-correlation energy is calculated with the generalized gradient approximation of Perdew-Wang (PW91).[36] The fractional occupancies are determined through the broadening approach of Methfessel and Paxton with N=1 and σ=0.1 eV.[37] The Brillouin zone integration is performed with a $5\times5\times1$ Monkhorst-Pack grid of special *k* points centered at the Γ-point.[38] The energy criteria for total energy self-consistency is 10^{-5} eV.

The (1×1) N-covered Ag(111) surface is modeled by a periodic six-layer slab (five layers of Ag and one layer of N) with a (2×2) unit cell in the plane parallel to the surface and a supercell vector of 24.08 Å along the surface normal direction (*z*-axis). The topmost layer corresponds to N atoms adsorbed on the fcc sites of the Ag(111) surface (see Figure 1). The supercell dimensions are chosen to guarantee negligible interactions among the gas N atoms in the neighboring cells and between the surface and the gas N atom, when the latter is located in the middle of the vacuum. The equilibrium surface geometry is obtained by allowing full relaxation of the three topmost layers until the forces on the core ions are below 0.02 eV/Å. The Ag-Ag interlayer distances remain almost unchanged with respect to the theoretical bulk value d_0 =2.41 Å, as indicated in Figure 1. The N-monolayer is 1.26 Å above the neighboring Ag layer. This distance is in accordance with the adsorption position of a single N atom on the pristine Ag(111) surface,[17] $z=1.20$ Å. No relaxation in the plane parallel to the surface is obtained in any of the layers.

Next, the DFT energy grid of the total system, i.e., the gas N and the N-covered Ag(111) surface is calculated for 15 (x,y) positions of the gas N atom, which are uniformly distributed over the surface unit cell (crosses in Figure 2). For each (x,y) position, the height of the gas N atom measured from the topmost Ag layer is varied from $z=-1.49$ Å to $z=6$ Å in intervals of 0.07 Å. At $z=6$ Å all the energy curves have steadily merged to the same asymptotic value that is taken as the zero reference energy for the PES of the gas N atom interacting with the N-covered Ag(111) surface. All these energies are calculated within the frozen surface approximation, that is, keeping

the slab atoms fixed at their equilibrium positions. Therefore, as the surface N atom is kept frozen, N_2 desorption processes are unaccounted for in the present calculations. In all the calculations the origin of heights, $z = 0$, is placed at the topmost Ag layer.

Calculation of the 3D adiabatic PES

Different interpolation methods have been developed in the last years to gain energy precision in the order of tens of meV and successfully applied to study the interaction of diatomic molecules and atoms with metal surfaces. The modified Shepard[39] and the corrugation reduction procedure (CRP)[40] have been respectively used in Refs.[4,41–45] and in Refs.[44,46–53] to study the interaction of H_2 and N_2 on various metal surfaces. Six-dimensional PESs of O_2 have been interpolated with the CRP in Refs.[54] and with the neural networks method[55,56] in Refs.,[10,11,56,57] for instance.

In the present work, the adiabatic PES is constructed by interpolating the *ab-initio* data with the 3D CRP.[40] The idea behind this procedure consists in reducing the typically large PES corrugation by subtracting from it the potential energy between the gas N atom and the nearest atoms in the surface. The resulting 3D energy surface exhibits a smoother dependence on the coordinates (x,y,z) that facilitates the 3D interpolation within the required accuracy for treating low energy gas-surface dynamics.

Briefly, the 3D potential energy V^{3D} is written as

$$V^{3D}(\mathbf{r}) = I^{3D}(\mathbf{r}) + \sum_{i=1}^{n_{\mathrm{N}ads}} V^{1D}_{\mathrm{NN}_{ads}}(|\mathbf{r}-\mathbf{r_i}|) + \sum_{i=1}^{n_{\mathrm{Ag}}} V^{1D}_{\mathrm{NAg}}(|\mathbf{r}-\mathbf{r_i}|) \tag{1}$$

where $V^{1D}_{\mathrm{NN}_{ads}}$ and V^{1D}_{NAg} are pair potentials describing the interaction between the impinging gas N atom with position $\mathbf{r} \equiv (x,y,z)$ and the *ith*-slab atom located at position $\mathbf{r_i} \equiv (x_i,y_i,z_i)$. The interactions of the gas N atom with the adsorbed N (N_{ads} in the following) and with the Ag atoms are so different that we have been forced to use different pair potentials in each case. In particular, we approximate the N-N_{ads} interaction by the DFT calculated potential of a N atom on top of the fcc site, where N_{ads} is located. In similar terms, the N-Ag interaction is approximated by

the DFT potential of a N atom on top of the Ag site. The sums on the right hand side of Eq. (1) run over all slab atoms that give a non zero contribution to $V^{1D}_{\mathrm{NN}_{ads},\mathrm{NAg}}$. In practice, we include in the summations the atoms from the first, second and third layers that lie within a distance $d <$ 6.0 Å from the projectile. The resulting interpolation function I^{3D} is a smooth function that can be easily interpolated over *x*, *y* and *z* through a third order 3D spline interpolation. We have checked the accuracy of the constructed 3D PES by comparing a set of 18 *ab-initio* values not used in the interpolation with interpolated results (see Figure 2). The errors are small ($5-15$ meV) in the parts of the configuration space that are likely to be visited by the simulations, e.g. at PES values below a few eV.

Classical trajectory calculations

Using the adiabatic 3D PES, atomic dynamics simulations have been carried out at two different levels by solving in both cases the classical equations of motion. In one case, we perform 3D dynamics calculations of the gas N atom in which the adiabatic and frozen surface approximations are strictly applied. We use a conventional Monte-Carlo sampling of the position of N over the surface and of the azimuthal incidence angle of the N beam. In the second set of simulations, we applied the generalized Langevin oscillator model (GLO) to include nonadiabatic effects that refer to energy exchange and dissipation between the gas atom and the lattice.[58,59] Following the implementation of Ref.,[60] the surface motion is represented by a 3D harmonic oscillator with mass equal to that of the Ag atom. Coupled to it there is a second 3D oscillator (*ghost* oscillator) acting as a thermal bath that keeps the surface at temperature $T_s = 300$ K. More precisely, the *ghost* oscillator is subject to friction and random forces related to each other through the second fluctuation-dissipation theorem. The friction force represents the energy dissipated from the surface to the bulk, while the random force assures the energy flow from the bulk to the surface due to the thermal vibrations of the lattice. Similar to Ref.,[61] the frequencies associated to the surface and the *ghost* oscillators are represented by the surface phonon frequencies close to the edges of the Ag(111) surface Brillouin zone, $\hbar\omega_x$=$\hbar\omega_y$=14 meV and $\hbar\omega_z$=9 meV.[62] Since we follow the formulation of Refs.[59,63] for

GLO, we take the value $\hbar\gamma_g = \pi\omega_D/6 = 10\,\mathrm{meV}$ for the damping matrix diagonal elements, where ω_D denotes the Debye frequency. In the GLO simulations, the initial conditions of the surface and *ghost* oscillators are also sampled through a conventional Monte-Carlo procedure that adjusts the initial positions and velocities to the nominal surface temperature. As we are dealing with a N-covered surface and N atoms have very different masses, we have also applied the GLO method taking m_{N} as the surface atom mass (see below).

In the present work, all the trajectories start with the N atom at z=5.6 Å from the Ag topmost layer. At this height, the potential energy is almost zero (≤ 2 meV). The outcome of each trajectory is classified as reflection if the atom reaches the starting distance z=5.6 Å with a positive z velocity or as trapping, if after 15 ps the atom is not reflected. If the atoms arrive at z=-0.5 Å with a negative velocity, it is regarded as absorbed. Absorption events are scarce, though, and typically found only for very high incident energies $E_i > 6\,\mathrm{eV}$.

As discussed below, when energy dissipation into lattice vibrations is allowed, the projectile can stabilise in the adsorption well that exists over the fcc site. To be more precise, adsorption events are defined using this criterion: the maximum integration time (15 ps) is reached, and the total energy of the system (incident N atom and surface) is $< -k_B T$. We recall that the atom has zero potential energy at $z \geq 6$ Å. We have checked that the adsorption results are unaffected if a lower integration time of 10 ps is used. The typical reflection times are below 1 ps.

Results and discussion

In this section we discuss the PES topography and the results obtained from classical molecular dynamics on that PES, under conditions that resemble the experimental ones. In particular, we begin by studying the angular dependence of the reflected atoms when an incident effusive beam of average energy $\langle E_i \rangle = 4.3\,\mathrm{eV}$ is used, a setting that has been successfully applied to explain N scattering off the clean Ag(111).[61,64] Then, in order to understand the details of the effusive beam results, we make a closer inspection of the energy dependence of monoenergetic reflected

trajectories. Finally, the dynamics of N adsorption are studied.

PES topography

Compared with the clean Ag(111), the adsorbed N strongly enhances the attractive character of the surface and induces further corrugation in the PES. The differences observed in the adsorption wells are clear examples of such changes. The 3D PES for N on a clean Ag(111) surface has wells of similar depths -2.03 eV and -1.92 eV at the *fcc* and *hcp* sites, respectively.[17] In contrast, the 3D PES of a N atom on a N-covered Ag(111) surface shows a very deep narrow well (a global minimum of -7.426 eV) at the *fcc* site at a height $z = 2.40$ Å, i.e. 1.14 Å above the N_{ads} adsorption site, while the positions around the *hcp* site remain a shallower attractive region of depth $\lesssim 3$ eV. Nevertheless, there is no local minimum as such at the *hcp* site itself. These features are observed in the PES bidimensional cuts at relevant z values shown in Figure 3. The global minimum turns rapidly into a strong repulsive region as soon as the impinging N atom moves towards lower z values. At heights $z = 1.60 - 2.00$ eV very narrow concentric attractive regions can be found in the PES around N_{ads}, that originate from the strong N-N interaction.

Dynamics of reflected atoms from a non-monoenergetic beam

The hyperthermal atomic beams used in the N scattering experiments are not monoenergetic.[12,13] Therefore, we have performed MD simulations considering an initial kinetic energy profile that has a FWHM as large as 5.4 eV and average value $\langle E_i \rangle = 4.3$ eV (see Figure 4 inset), which nicely matches the experimental effusive beam energy spectrum. A total number of trajectories $N_{tot} = 3 \times 10^5$ has been used in order to obtain converged statistical averages. In the simulations, the incident polar angle of all incident atoms is kept fixed at $\Theta_i = 60^\circ$, and a random azimuthal angle Φ_i is chosen for each atomic trajectory. We have checked that the incidence azimuth does not play a determinant role in the dynamics. Figure 4 shows the polar angular distribution, I_R, for the N atoms that undergo in-plane scattering ($\Phi_f \simeq \Phi_i$) in adiabatic and GLO dynamics. Each data point of this graph is actually contributed by the number N of reflected atoms contained within

an acceptance angle $\delta = 4^\circ$. By doing this, the distribution is represented as if a circular atom detector of angular aperture δ were placed at the direction defined by the pair of angles (Θ_f, Φ_i). The criterion provided by this pair of angles and δ yields the conditions for an atom to undergo in-plane scattering and to be detected at a given polar angle Θ_f. Afterwards, the distributions are normalised to N_{tot}. Hence, we define the in-plane reflected intensities as follows:

$$I_R(\Theta_f) = \frac{N(\Theta_f)}{N_{tot}\Delta\Theta_f} \tag{2}$$

where $\Delta\Theta_f = 8^\circ$ is the polar angle interval spanned by the detector aperture. As the experimental detector aperture is slightly smaller, of 1.6°, we have checked that the distributions are not significantly altered by the use of tolerances $\delta < 4^\circ$, albeit a smaller signal-to-noise ratio is achieved for $\delta = 4^\circ$. Both adiabatic and GLO dynamics result in broad $I_R(\Theta_f)$ curves, as shown in Figure 4, that take their maximum values at outgoing polar angles Θ_f lying close to the specular direction, namely $\Theta_f \lesssim 60^\circ$ for the adiabatic case and $\Theta_f \gtrsim 60^\circ$ for the GLO case.

The experimental reflected atomic distributions found by Ueta *et al.* are similar for the clean and N-covered Ag(111) surfaces.[12,13] The distribution profiles consist of a broad background and a sharp peak superimposed onto it at the specular direction. Energy exchange with the lattice has a relevant role in the reflection dynamics. In fact, our GLO theoretical distribution is in good qualitative agreement with the experimental data, while agreement with the adiabatic one is poorer, as observed in Figure 4. It is noteworthy that the profiles obtained from the PES of clean and N-covered Ag(111) surfaces resemble each other, despite the PES themselves having little in common.[17,64] Both of them have strongly corrugated topographies, but the global minimum is 5.40 eV deeper in the N-covered PES. The much more attractive character of the N-covered surface PES does not seem to come through in the reflected spectrum. The broad background arises as a consequence of the corrugated energy landscape, and it seems to be quite insensitive to the particular details of the PES, such as well depths.

Regarding the sharp experimental specular peak in the distribution, Ueta *et al.* have attributed it

to scattering of excited N atoms.[12,13] A fraction of the N atoms in the experimental beam is known to be out of the ground state,[12] and the PES dictating the reflection of such species is expected to be more repulsive.[65] Our simulations for ground state N atoms do not yield such a sharp peak and hence support the presence of excited atoms in the experiment.

In addition to the angular distributions, Ueta *et al* measure the final kinetic energy of the reflected N atoms.[13] In the experiments, the atoms that are reflected close to the surface normal have a final-to-initial energy ratio of $\langle E_f \rangle / \langle E_i \rangle \simeq 0.60 - 0.70$, whereas at $\Theta_f > 70^\circ$ it is found that $\langle E_f \rangle / \langle E_i \rangle > 1$, and this occurs for N scattering off both the clean and the N-covered surfaces.[12,13] Indeed, the experimental $\langle E_f \rangle / \langle E_i \rangle$ dependence with Θ_f in the N-covered and clean Ag(111) surfaces are almost a perfect match. It has been theoretically proved that the difference between the scattering properties at low and high kinetic energies of the N atoms is crucial to explain the $\langle E_f \rangle / \langle E_i \rangle > 1$ values for scattering off a clean Ag(111) surface.[61] In fact, MD simulations show that this behaviour can be nicely explained even in the absence of energy exchange with the surface, i.e. it is purely a *trajectory effect* and it has its origin in the non-monoenergetic character of the incident beam, albeit quantitative agreement with the experiment is better when GLO is introduced in the dynamics.[61] This trajectory effect observed in the clean surface consists in atoms with different E_i being scattered at different polar angles, regardless of the inelastic character of the atom-surface collision.

Interestingly, the interpretation described above for the clean Ag(111) is not applicable to the N-covered one. Figure 5 shows the final-to-initial average kinetic energy ratio values, $\langle E_f \rangle / \langle E_i \rangle$, obtained from our simulations. Neither the adiabatic one nor the GLO one reproduce the $\langle E_f \rangle / \langle E_i \rangle > 1$ behaviour observed experimentally for grazing outgoing atoms. Indeed, the adiabatic MD shows an energy ratio decrease with increasing Θ_f that totally rules out the trajectory effect already observed on the clean Ag(111). The experimental energy ratios cannot be explained by the energy exchange with the surface neither: the use of GLO in the simulations results in an almost constant $\langle E_f \rangle / \langle E_i \rangle \simeq 0.7$. It could be argued that the GLO implementation used here is not accurate enough, since it assumes that only atoms with the Ag atom mass, m_{Ag}, are present in the Langevin

oscillator. Nevertheless, the substitution of the topmost atom masses m_{Ag} by smaller masses m_{N} would not improve the agreement with the experiment, as the energy dissipated into lattice vibrations would be larger overall, due to the use of a lighter and "softer" oscillator, thus resulting in even smaller $\langle E_f \rangle / \langle E_i \rangle$ values.

In summary, the MD simulations shown above, featuring an effusive beam and energy dissipation through lattice vibrations, reproduce nicely the experimental $I_R(\Theta_f)$ profile (except for the excited states peak, which is beyond the scope of the present work). The reflected in-plane N atom distribution seems to be rather insensitive to the PES details. Notwithstanding, the scattered atomic energy distributions do have a non-trivial dependence on the PES details and the MD analyses, which are shown in Figure 5, do not fully account for the experimental $\langle E_f \rangle / \langle E_i \rangle$ behaviour. The ab-initio calculated energies and the CRP interpolation procedure used in the present work ensure a good quality 3D PES. We will show that both the scattering angle distributions and the $\langle E_f \rangle / \langle E_i \rangle$ ratio are perfectly consistent with the PES characteristics. The discrepancies with the experimental data can be explained as a different N coverage.

Trajectory analysis of monoenergetic beams I: reflection

In order to understand the simulated $\langle E_f \rangle / \langle E_i \rangle$ ratios of Figure 5, we have performed detailed analyses of the MD trajectories at well defined atomic kinetic energies, E_i, with $\Theta_i = 60^\circ$ and a random Φ_i distribution. Statistical averages have been obtained over $N_{tot} = 3 \times 10^4$ trajectories for each E_i value.

The reflection dynamics of atomic N can be understood as a combination of a trajectory effect and the energy lost by the atoms upon collision with the surface. To account for the former, we have performed simulations under adiabatic conditions, i.e. $E_f / E_i = 1$. Figure 6 shows the obtained in-plane angular distributions of reflected N atoms, $I_R(\Theta_f; E_i)$, for a set of E_i values ranging from 0.3 to 10.0 eV. For $E_i > 3.0$ eV, broad distributions are obtained. For $E_i < 3.0$ eV, the distributions consist of a broad background and a sharper peak superimposed onto it at the specular $\Theta_f = 60^\circ$ direction. The detailed analysis of the trajectories shows that most slow atoms that are reflected

in-plane interact with the repulsive regions of the PES that lie far from the surface and are located around N_{ads} at heights $z \simeq 2.00$ Å (see Figure 3). Figure 7 shows the $I_R(\Theta_f; E_i)$ distributions resolved by depth, i.e. at a given E_i and angle Θ_f, each intensity of the plot accounts for the number of reflected atoms that reach a range of z_{min} values, where z_{min} represents the minimum height reached by the incident N along its trajectory. Only two representative cases of the low and high energy scenarios, $E_i = 1.3, 4.3$ eV, are shown in the figure for the sake of simplicity. For both E_i values, we observe that the distribution at the specular Θ_f range is contributed mainly by N atoms scattered from high z_{min}, whilst atoms from low z_{min} leave the surface close to the normal. In the $E_i = 1.3$ eV panel, we see that scattering from $z_{min} > 1.60$ Å values clearly dominates. Only a few atoms are reflected from $z_{min} < 1.60$ Å that yield broad angular distributions. This results in the sharp peak superimposed onto a broad profile observed in the $E_i = 1.3$ eV curve of Figure 6. In contrast, for $E_i = 4.3$ eV, contributions of atoms from both low and high z_{min} are similar in magnitude, which results in an overall broad profile (see the $E_i = 4.3$ eV curve of Figure 6). This is due to the fact that faster atoms can penetrate deeper in the surface. This is, these atoms reach lower z_{min} values and can explore vaster regions of the PES, such as the *hcp* region of the unit cell, which is shallow but rapidly varying in energies. Thus, scattering off those regions will follow highly unpredictable trajectories.

The analysis of the number of rebounds experienced by the reflected N allows us to gain further insight in the low energy regime. The insets of Figure 6 show the average number of rebounds in the in-plane reflected trajectories, $\langle N_r \rangle$. A rebound in the trajectory is defined as a sign change from negative to positive in the perpendicular component of the atomic velocity, this is, N_r indicates the number of collisions with the surface. For most Θ_f and E_i values, we find $\langle N_r \rangle \simeq 2$. An exception occurs for the lowest E_i values at $\Theta_f < 45°$, where the N atoms leave the surface after $\langle N_r \rangle \simeq 6$ rebounds. When atoms suffer several rebounds, they are less likely to continue along the specular trajectory and they are reflected at less predictable directions, yielding non-negligible reflected intensities at low Θ_f angles, i.e. closer to the surface normal.

The N atoms within the effusive beam have energies that differ as much as $\gtrsim 3$ eV from the

average value $\langle E_i \rangle = 4.3\,\text{eV}$. According to the analysis above, the most energetic atoms within the beam will be preferentially scattered at angles $\Theta_f < 60^\circ$, while the least energetic ones will undergo nearly specular reflection. As a result, the angular dependence of the value $\langle E_f \rangle / \langle E_i \rangle$, shown in Figure 5 for the adiabatic case, decreases as a function of Θ_f. Interestingly, this result is in contrast with the distribution obtained for N scattering off clean Ag(111), where the atoms with higher E_i are reflected at large Θ_f values, while the slowest atoms yield a broad angular spectra. For this reason, the trajectory effect suffices to explain the increase in the ratio $\langle E_f \rangle / \langle E_i \rangle$ at large Θ_f angles of the atoms reflected off the clean Ag(111) surface,[61,64] but not off the N-covered case, where, on the contrary, it predicts a decreasing behaviour.

When GLO is used in the simulations, this is, when we allow the N atoms to transfer energy into lattice vibrations, the $I_R(\Theta_f; E_i)$ distributions depend on E_i essentially in the same way as the adiabatic ones, as it can be seen by comparing Figure 8 and Figure 6. We observe that the N atoms with lower E_i are scattered mainly at specular directions, while the atomic distributions for faster atoms are broad. Therefore, the trajectory effect discussed above remains a significant feature of the reflection dynamics even when energy dissipation into lattice vibrations is considered within the simulations. The main consequence of non-adiabatic effects is found at low E_i and $\Theta_f < 45^\circ$, where the observed intensities are lower than the corresponding adiabatic ones, thus providing a better agreement with the experiments. In order to understand this, we examine the z_{min}-resolved $I_R(\Theta_f; E_i)$ curves in the GLO case for $E_i = 1.3, 4.3\,\text{eV}$, which are shown in Figure 9. The addition of the dissipation channel has a dramatic impact on the reflection dynamics of atoms with $E_i = 1.3\,\text{eV}$, as only a handful of them reach low z_{min} regions of the surface. As we will show in detail in the next section, the reason is that most of the atoms reaching low z_{min} in the adiabatic simulations end up adsorbed on the surface when energy dissipation is allowed. As a result, almost every N atom is scattered off the surface at distances above 2.00 Å. Similarly to the adiabatic calculations, these atoms are responsible for the peak at the specular outgoing angle seen in the $E_i = 1.3\,\text{eV}$ curve of Figure 8. Energy dissipation affects the $E_i = 4.3\,\text{eV}$ angular distributions less significantly and, indeed, many similarities can be observed in the histograms of Figure 9 and

Figure 7 for that energy.

Next, we focus on the final-to-initial energy ratio obtained with the GLO simulations. As discussed above, the angular distribution profiles depend strongly on the E_i values, as they are broader for larger E_i. In contrast, the energy loss behaviour, which is shown in the insets of Figure 8, follows the same trend for all the studied E_i values. The atoms that scatter off at $\Theta_f = 0$ suffer a significant energy loss, as shown by the average values $\langle E_f \rangle / E_i \simeq 0.5$, decreasing monotonically with Θ_f to average losses of 20%. This observation on the energy, combined with the behaviour of I_R as a function of E_i, allows us to understand why the $\langle E_f \rangle / \langle E_i \rangle$ distribution in the effusive beam simulation with GLO does not substantially vary with Θ_f (see Figure 5). The slowest particles in the beam are reflected preferentially at specular directions with $\Theta_f \simeq 60$, but the atoms outgoing at such angles lose on average only 20% of their initial energy upon collision with the surface. In contrast, the fastest atoms, which are predominant at low Θ_f values, experience larger energy losses of 50%. When adding up these two effects, the result is a nearly constant ratio $\langle E_f \rangle / E_i \simeq 0.7$, as seen in the GLO curve of Figure 5.

We have previously explained the theoretical in-plane reflection spectra for a effusive beam. Nevertheless, the in-plane spectra shown so far in the present paper account for a small fraction of the total number of reflected atoms only. Most trajectories are subject to out-of-plane scattering and the actual global distribution of reflected atoms is also broad over Φ_f angles. In fact, the trajectory analysis at all outgoing azimuthal directions, Φ_f, reveals that the atoms with small E_i are reflected within a cone around the specular direction. For example, for $E_i = 1.3\,\text{eV}$, the distribution has an approximate FWHM of 40° both in Θ_f and Φ_f. An in-plane spectrum captures a section of this narrow cone, but cannot yield information of the other Φ_f directions. Conversely, the distributions of faster atoms are broad in Θ_f and Φ_f. A simple inspection of the in-plane reflection distributions with GLO (see Figure 8) would suggest that more atoms are reflected off the surface at, say, $E_i = 2.3\,\text{eV}$ than at $E_i = 6.3\,\text{eV}$. However, the perspective changes when all the trajectories, and not only the in-plane reflected ones, are considered. By doing so, we realize that most slowly incident atoms end up being trapped by the surface. This is shown in the the sticking probability

of the N-covered Ag(111) surface (Figure 10), which increases rapidly at low E_i.

Another example of the limitations in the picture offered by the in-plane analyses is found in the average number of rebounds, $\langle N_r \rangle$, undergone by the reflection trajectories. The $\langle N_r \rangle$ values shown in the inset of Figure 10 include in-plane as well as out-of-plane trajectories. Due to the energy loss channel, the slow atoms that undergo more than two rebounds do not keep enough kinetic energy to leave the surface and end up being adsorbed in the wells of the PES. The $\langle N_r \rangle$ values of the adiabatic case are also shown in the Figure 10 inset for comparison. Interestingly, they take much higher values at low E_i if out-of-plane trajectories are included in the average. For example, we find values as large as $\langle N_r \rangle = 19$ for $E_i = 0.3\,\text{eV}$ in Figure 10, while the maximum value drops to $\langle N_r \rangle = 7$ when only in-plane trajectories are considered (the latter value corresponds to outgoing trajectories along the normal in the inset of Figure 6).

Trajectory analysis of monoenergetic beams II: adsorption

The careful analysis of the reflected N atoms has revealed why the in-plane angular distributions are rather similar upon scattering on the clean and N-covered Ag(111) but the final-to-inital energy distributions are not. Now, the question is to understand the origin of the discrepancy between the experimental and theoretical energy distributions at grazing outgoing angles. As discussed in this section, the N adsorption events predicted in the GLO simulations at low incident energies (see Figure 10) can provide a reasonable explanation. A closer inspection of the final positions in the trajectories of these atoms shows that these end up apparently bound at positions around the N_{ads} site (see Figure 10 inset), at distances close to the N_2 molecule bondlength, i.e. at the deep adsorption well discussed above. The large binding energy at that site suggests, indeed, that a molecule is being formed on the surface. However, we have checked that no molecular adsorption well is found in the DFT-based six-dimensional PES of N_2 interacting with the clean Ag(111) surface. Hence, molecular adsorption of N_2 on N-covered Ag(111) is not expected, neither, and we infer that the N_2 molecules formed on the surface will eventually desorb, although the rigid character of the 3D atomic PES does not allow the N_{ads} atom to shift from its surface position.

The atomic adsorption energy at the fcc site is $E_{ads} = 7.426\,\mathrm{eV}$ on the N-covered surface, and $2.03\,\mathrm{eV}$ on the clean one. The energy needed to release both projectile and surface N_{ads} atom can be provided by the formation of a N_2 molecule, a process that typically releases $9.8\,\mathrm{eV}$ in the gas phase. An excess kinetic energy hinders the efficiency of this process, as it reduces the sticking probability (see Figure 10). This energy argument strongly supports the interpretation of adsorption events in the MD runs as pick-up reactions resulting in N_2 molecules. This tendency towards adsorption on the N-covered Ag(111) is also manifested in the adiabatic calculations, where the low energy N atoms undergo many rebounds before being reflected due to the strong attractive character of the surface (see Figure 10 inset).

This interpretation of adsorption processes as pick-up events provides the following explanation for the very subtle differences observed by Ueta *et al.* between the clean and the N-covered surfaces.[13] Due to the highly efficient pick-up process, it is expected that the effective surface coverage probed by the N projectiles is the outcome of a highly dynamical mechanism. In principle, one should consider the kinetics of a steady adsorption and removal of N. Since the sticking (i.e. pick-up reaction) probability of N on the (1×1) covered surface is considerable larger than the adsorption probability on the clean surface,[17] it is very reasonable to infer that not all the fcc sites are occupied by N_{ads} atoms at the experimental saturation coverage conditions. Therefore, the experimental scattering properties of the sample would appear to be dominated by the clean regions, resulting in an energy loss spectrum very similar to that observed in clean Ag(111).

There are other fine experimental details that further support surface cleaning by a pick-up reaction. These details are to be found in the angular intensity distribution of N_2 molecules scattering in-plane off N-covered and clean Ag(111), shown in Ref.[13] On both surfaces N_2 is strongly repelled and a sharp specular peak is observed. Whilst the amount of reflected molecules at low Θ_f angles in the clean surface is almost negligible, a small, yet non-negligible, intensity is registered off the N-covered surface at $\Theta_f \lesssim 40^\circ$. The latter molecules are attributed to the recombination of N_{ads} with the N atoms present in the incident molecular beam, that is superimposed onto the regular N_2 scattering component. The presence of the two N_2 components is also evidenced in

the time-of-flight spectra, that are better explained if two groups of molecules are considered that leave the surface at different velocities.

Conclusions

In the present work, we have constructed an ab-initio calculated 3D PES for an N atom interacting with a N-covered Ag(111) surface, and we have analyzed the scattering properties by means of classical MD. The molecular beams experiments of hyperthermal N atoms scattering off clean and N-covered Ag(111) surfaces performed by Ueta *et al.* suggest that the energy landscapes of Ag(111) should not be significantly altered by the adsorbed N species, as the in-plane scattered atomic distributions and the final-to-initial energy ratios show similar profiles as a function of the outgoing polar angle.[13] In contrast with this interpretation, we find huge differences between this PES and that of the clean surface that, strikingly, do not have a noticeable impact on the angular atomic distributions. In fact, when an energy loss channel associated to lattice vibrations is introduced, the quantitative agreement with the experiment is remarkable. The energy ratios are altered, though, and are in discrepancy with the experimental ones at grazing outgoing angles. These theoretical results on the N-covered Ag(111) surface can be rationalised in terms of the corrugated topography of the PES. The analysis of the dynamics of adsorption puts forward another interpretation of the experiment, namely that N_2 molecules are formed by a pick-up reaction, resulting in clean Ag regions on the surface. Albeit the constraints in the present calculations do not allow desorption of the molecular species, this hypothesis is supported by indirect experimental evidence of such a reaction mechanism being active during the dosing of N atoms.

It is still to be proved by direct means whether surface N pick-up events are readily taking place. Despite the measurements and the simulations with a 3D PES point clearly towards a gas-surface reaction, a higher dimensional model would be needed to unequivocally account for the "pick up" phenomenon. This would be an unusual N_2 formation mechanism by molecular beams experiments. Typically, molecule formation by abstraction of adsorbed atoms using atomic beams

involves hydrogen species, as reported for example in Refs.[25–29] In this respect, details such as the Eley-Rideal or hot-atom nature of the N_2 pick-up process remain also a matter of study, both experimentally and theoretically. Another point that would require future analysis is the N_2 recombination kinetics. Since the large sticking probabilities at low incident energies suggest that N_2 formation is a highly efficient mechanism, it might non trivially affect the equilibrium N coverage under experimental conditions.

Acknowledgement

We thank G.A. Bocan, P. Larregaray and A.W. Kleyn for stimulating discussions. M.B.-R. acknowledges financial support from the Gipuzkoako Foru Aldundia and the European Union 7th Framework Programme (FP7/2007-2013) under grant agreement no. FP7-PEOPLE-2010-RG276921. Work also supported by the Gobierno Vasco-UPV/EHU project IT-366-07, and the Spanish MICINN project FIS2010-19609-C02-02. Computational resources were provided by the DIPC computing center.

References

(1) Groß, A.; Scheffler, M. *Phys. Rev. B* **1998**, *57*, 2493–2506.

(2) Busnengo, H. F.; Dong, W.; Salin, A. *Phys. Rev. Lett* **2004**, *93*, 236103.

(3) Alducin, M.; Muino, R. D.; Busnengo, H. F.; Salin, A. *Phys. Rev. Lett* **2006**, *97*, 056102.

(4) Díaz, C.; Vincent, J. K.; Krishnamohan, G. P.; Olsen, R. A.; Kroes, G. J.; Honkala, K.; Norskøv, J. K. *Phys. Rev. Lett.* **2006**, *96*, 096102.

(5) Nieto, P.; Pijper, E.; Barredo, D.; Laurent, G.; Olsen, R. A.; Baerends, E.-J.; Kroes, G.-J.; Farías, D. *Science* **2006**, *312*, 86–89.

(6) Salin, A. *J. Chem. Phys.* **2006**, *124*, 104704.

(7) Díaz, C.; Pijper, E.; Olsen, R. A.; Busnengo, H. F.; Auerbach, D.; Kroes, G. J. *Science* **2009**, *326*, 832–834.

(8) Groß, A. *ChemPhysChem* **2010**, *11*, 1374–1381.

(9) Geethalakshmi, K. R.; Juaristi, J. I.; Díez Muiño, R.; Alducin, M. *Phys. Chem. Chem. Phys.* **2011**, *13*, 4357–4364.

(10) Meyer, J.; Reuter, K. *New J. Phys.* **2011**, *13*, 085010.

(11) Goikoetxea, I.; Beltran, J.; Meyer, J.; Juaristi, J. I.; Alducin, M.; Reuter, K. *New J. Phys.* **2012**, *14*, 013050.

(12) Ueta, H.; Gleeson, M. A.; Kleyn, A. W. *J. Phys. Chem. A* **2009**, *113*, 15092–15099.

(13) Ueta, H.; Gleeson, M. A.; Kleyn, A. W. *J. Chem. Phys.* **2011**, *135*, 074702.

(14) Sitz, G. O.; Kummel, A. C.; Zare, R. N. *J. Chem. Phys.* **1987**, *87*, 3247–3249.

(15) Sitz, G. O.; Kummel, A. C.; Zare, R. N.; Tully, J. C. *J. Chem. Phys.* **1988**, *89*, 2558–2571.

(16) Sitz, G. O.; Kummel, A. C.; Zare, R. N.; Tully, J. C. *J. Chem. Phys.* **1988**, *89*, 2572–2582.

(17) Martin-Gondre, L.; Bocan, G. A.; Alducin, M.; Juaristi, J. I.; Díez Muiño, R. *Comp. Theo. Chem.* **2012**, *990*, 126–131.

(18) Ueta, H.; Groot, I. M.; Gleeson, M. A.; Stolte, S.; McBane, G. C.; Juurlink, L. B.; Kleyn, A. W. *ChemPhysChem* **2008**, *9*, 2372–2378.

(19) Wei, C.; Groß, A.; Scheffler, M. *Phys. Rev. B* **1998**, *57*, 15572–15584.

(20) Groß, A.; Wei, C.; Scheffler, M. *Surf. Sci.* **1998**, *416*, L1095–L1100.

(21) Groß, A.; Scheffler, M. *Phys. Rev. B* **2000**, *61*, 8425–8432.

(22) Lozano, A.; Groß, A.; Busnengo, H. F. *Phys. Rev. B* **2010**, *81*, 121402.

(23) Groß, A. *J. Chem. Phys.* **2011**, *135*, 174707.

(24) Lykke, K.; Kay, B. D. *SPIE Proc.* **1990**, *1208*, 18–29.

(25) Rettner, C. T. *Phys. Rev. Lett.* **1992**, *69*, 383–386.

(26) Rettner, C. T.; Auerbach, D. J. *Phys. Rev. Lett.* **1995**, *74*, 4551–4554.

(27) Rettner, C. T.; Auerbach, D. J. *Science* **1994**, *263*, 365–367.

(28) Rettner, C. T. *J. Chem. Phys.* **1994**, *101*, 1529–1546.

(29) Rettner, C. T.; Auerbach, D. J.; Lee, J. *J. Chem. Phys.* **1996**, *105*, 10115–10122.

(30) Lemoine, D.; Quattrucci, J. G.; Jackson, B. *Phys. Rev. Lett.* **2002**, *89*, 268302.

(31) Ree, J.; Kim, Y. H.; Shin, H. K. *J. Chem. Phys.* **1996**, *104*, 742–757.

(32) Wheeler, M. C.; Seets, D. C.; Mullins, C. B. *J. Chem. Phys.* **1997**, *107*, 1672–1675.

(33) Groß, A.; Dianat, A. *Phys. Rev. Lett.* **2007**, *98*, 206107.

(34) Kresse, G.; Hafner, J. *Phys. Rev. B* **1993**, *47*, 558–561.

(35) Vanderbilt, D. *Phys. Rev. B* **1990**, *41*, 7892–7895.

(36) Perdew, J. P.; Chevary, J. A.; Vosko, S. H.; Jackson, K. A.; Pederson, M. R.; Singh, D. J.; Fiolhais, C. *Phys. Rev. B* **1992**, *46*, 6671–6687.

(37) Methfessel, M.; Paxton, A. T. *Phys. Rev. B* **1989**, *40*, 3616–3621.

(38) Monkhorst, H. J.; Pack, J. D. *Phys. Rev. B* **1976**, *13*, 5188–5192.

(39) Ischtwan, J.; Collins, M. A. *J. Chem. Phys.* **1994**, *100*, 8080–8088.

(40) Busnengo, H. F.; Salin, A.; Dong, W. *J. Chem. Phys.* **2000**, *112*, 7641–7651.

(41) Crespos, C.; Collins, M. A.; Pijper, E.; Kroes, G. J. *Chem. Phys. Lett.* **2003**, *376*, 566–575.

(42) Crespos, C.; Collins, M. A.; Pijper, E.; Kroes, G. J. *J. Chem. Phys.* **2004**, *120*, 2392–2404.

(43) Abufager, P.; Crespos, C.; Busnengo, H. *Phys. Chem. Chem. Phys* **2007**, *9*, 2258–65.

(44) Díaz, C.; Olsen, R. A.; Busnengo, H. F.; Kroes, G. J. *J. Phys. Chem. C* **2010**, *114*, 11192–11201.

(45) Chen, J.-C.; Juanes-Marcos, J. C.; Woittequand, S.; Somers, M. F.; Díaz, C.; Olsen, R. A.; Kroes, G.-J. *J. Chem. Phys.* **2011**, *134*, 114708.

(46) Busnengo, H. F.; Dong, W.; Salin, A. *Chem. Phys. Lett.* **2000**, *320*, 328–334.

(47) Olsen, R. A.; Busnengo, H. F.; Salin, A.; Somers, M. F.; Kroes, G. J.; Baerends, E. J. *J. Chem. Phys.* **2002**, *116*, 3841–3855.

(48) di Césare, M. A.; Busnengo, H. F.; Dong, W.; Salin, A. *J. Chem. Phys.* **2003**, *118*, 11226–11234.

(49) Riviere, P.; Busnengo, H. F.; Martin, F. *J. Chem. Phys.* **2004**, *121*, 751–760.

(50) Laurent, G.; Martin, F.; Busnengo, H. F. *Phys. Chem. Chem. Phys* **2009**, *11*, 7303–7311.

(51) Volpilhac, G.; Salin, A. *Surf. Sci.* **2004**, *556*, 129–144.

(52) Alducin, M.; Díez Muiño, R.; Busnengo, H. F.; Salin, A. *J. Chem. Phys.* **2006**, *125*, 144705.

(53) Goikoetxea, I.; Alducin, M.; Díez Muiño, R.; Juaristi, J. I. *Phys. Chem. Chem. Phys.* **2012**, *14*, 7471–7480.

(54) Alducin, M.; Busnengo, H. F.; Muiño, R. D. *J. Chem. Phys.* **2008**, *129*, 224702.

(55) Lorenz, S.; Groß, A.; Scheffler, M. *Chem. Phys. Lett.* **2004**, *395*, 210–215.

(56) Behler, J.; Lorenz, S.; Reuter, K. *J. Chem. Phys.* **2007**, *127*, 014705.

(57) Behler, J.; Delley, B.; Lorenz, S.; Reuter, K.; Scheffler, M. *Phys. Rev. Lett.* **2005**, *94*, 036104.

(58) Adelman, S. A. *J. Chem. Phys.* **1979**, *71*, 4471–4486.

(59) Tully, J. C. *J. Chem. Phys.* **1980**, *73*, 1975–1985.

(60) Busnengo, H. F.; di Césare, M. A.; Dong, W.; Salin, A. *Phys. Rev. B* **2005**, *72*, 125411.

(61) Martin-Gondre, L.; Alducin, M.; Bocan, G. A.; Díez Muiño, R.; Juaristi, J. I. *Phys. Rev. Lett.* **2012**, *108*, 096101.

(62) Ponjée, M. W. G.; Flipse, F. J.; Denier van der Gon, A. W.; Brongersma, H. H. *Phys. Rev. B* **2003**, *67*, 174301.

(63) Adelman, S. A.; Doll, J. D. *J. Chem. Phys.* **1976**, *64*, 2375–2388.

(64) Martin-Gondre, L.; Bocan, G. A.; Blanco-Rey, M.; Alducin, M.; Juaristi, J. I.; Díez Muiño, R. *(in preparation)* **2012**.

(65) Kokh, D. B.; Buenker, R. J.; Whitten, J. L. *Surf. Sci.* **2006**, *600*, 5104–5113.

Figure 1: Sphere model of the N-covered Ag(111) surface. Small turquoise spheres represent N atoms and large spheres represent Ag atoms. The origin of z coordinates is placed at the topmost Ag layer (white spheres). The maximum N coverage is considered in this work, that consists of a N atom at each fcc site of the surface (on top of the third Ag layer positions) and thus results in a (1×1) lateral periodicity with lattice parameter $a_0 = 2.95$ Å. The (1×1) unit cell is depicted by a dashed line.

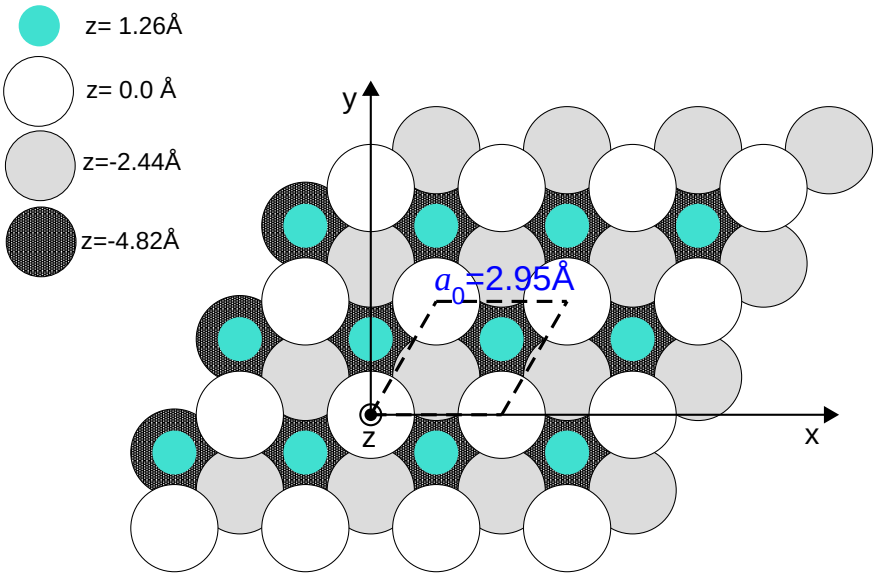

Figure 2: Quality tests of the CRP interpolated PES. In the insets, the small black crosses indicate the (x,y) coordinates used to construct the PES (there are 15 symmetry inequivalent points), and the large symbols label a few relevant coordinates out of the 18 (x,y) points used to test the PES. The curves on the top and bottom panels show the potential energies as a function of height z for the test coordinates in the *hcp* and fcc regions of the (1×1) cell, respectively. The values obtained from CRP interpolation are represented by lines and the symbols correspond to the energies obtained directly from DFT.

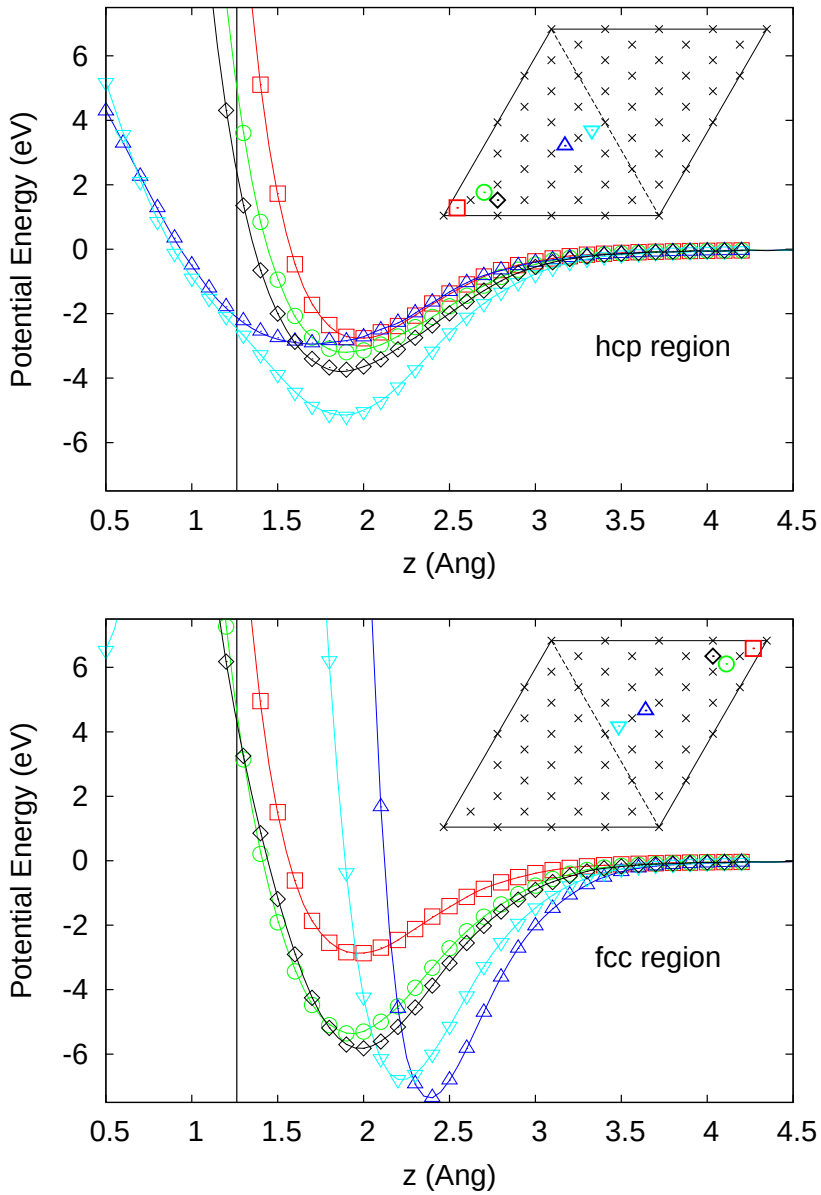

Figure 3: Bidimensional contour maps that result from cutting the interpolated 3D PES in the (1×1) unit cell (see Figure 1) at different heights z of the gas N atom. The value $z = 2.40$ Å is the distance at which the global minimum at the fcc hollow is found. The minimum value $z = 1.26$ Å coincides with the height of the adsorbed N (fcc hollow). The intermediate z values show the rapid evolution of the 3D PES from very attractive (dark blue) to strongly repulsive (yellow) as the gas N approaches the adsorbed N atom. The zero potential energy (PE) value is marked by a thick black line. Dashed white (thin black) contour lines indicate negative (positive) PE values separated in intervals of 0.5 eV (2.0 eV).

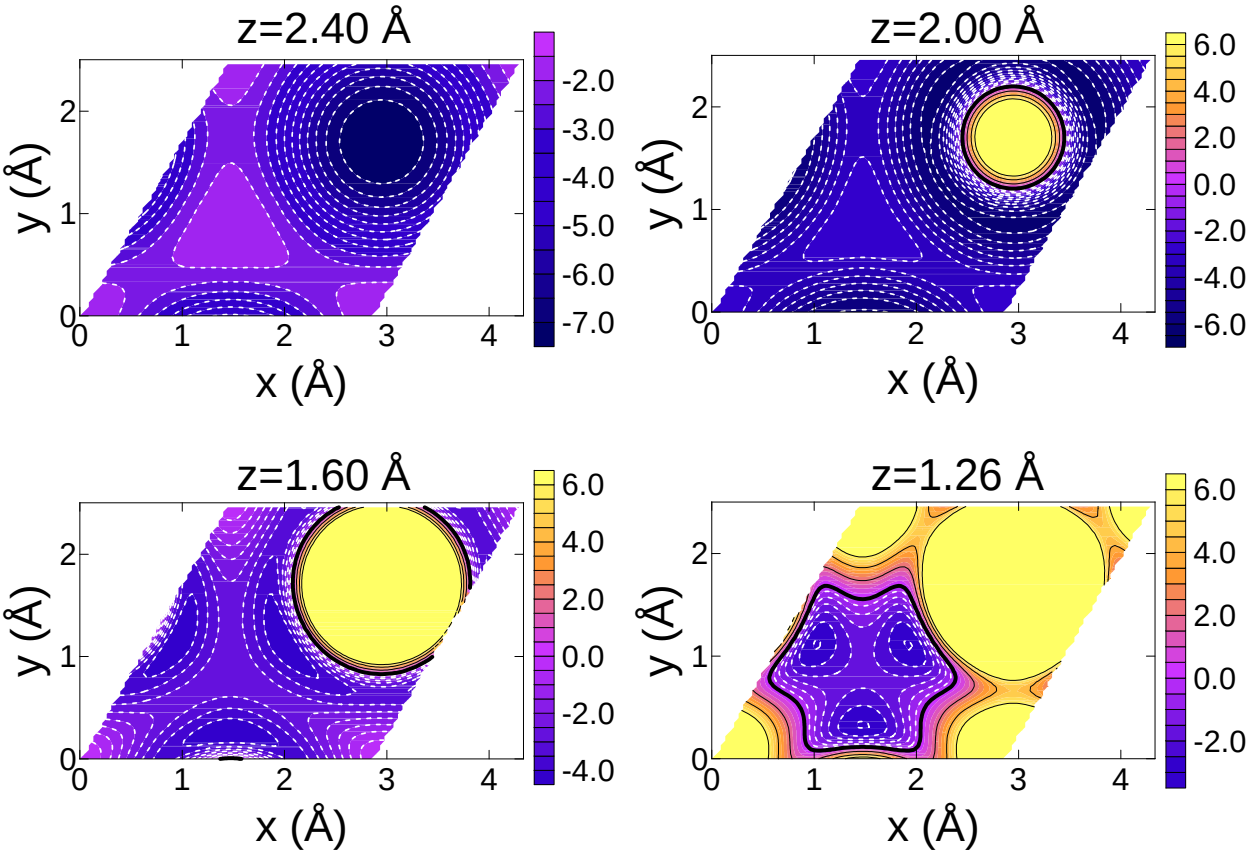

Figure 4: Polar angle distribution of in-plane reflected N atoms from a effusive beam scattered off N-covered Ag(111). The inset shows the kinetic energy distribution of the incident beam. The theoretical GLO (squares) and adiabatic (circles) curves are shown. For comparison purposes, the experimental data (large triangles) have been normalised to yield an area under the curve that matches either the area under the GLO curve (empty triangles) or the adiabatic one (filled triangles).

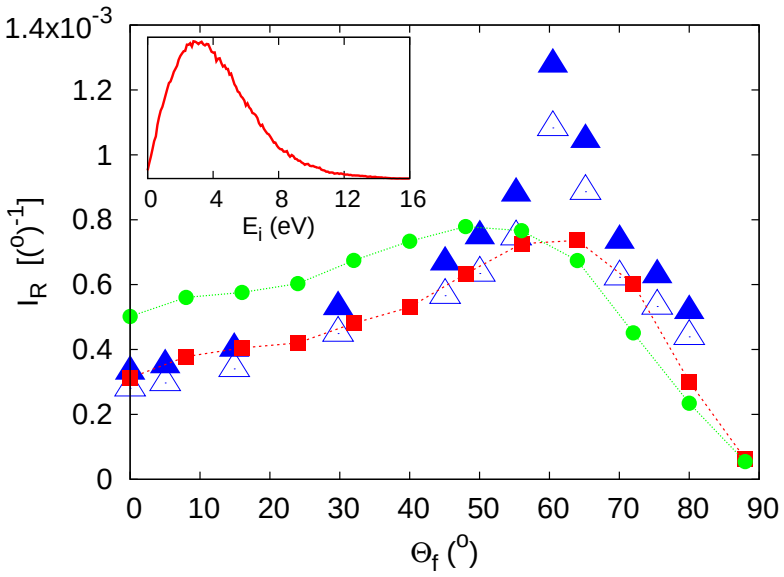

Figure 5: Ratio of in-plane final-to-initial average energy of the reflected N atoms of Figure 4. Symbols are as in Figure 4.

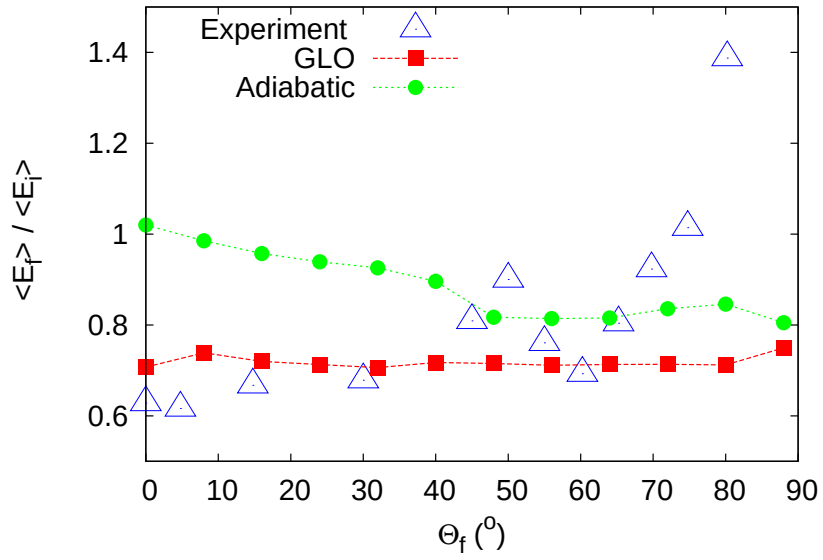

Figure 6: Polar angle distribution of in-plane reflected mono-energetic N atoms under adiabatic conditions for individual incident energies E_i. Top and bottom panels show high and low energy regimes, respectively. The insets show the average number of rebounds $\langle N_r \rangle$ undergone by the atoms upon in-plane reflection.

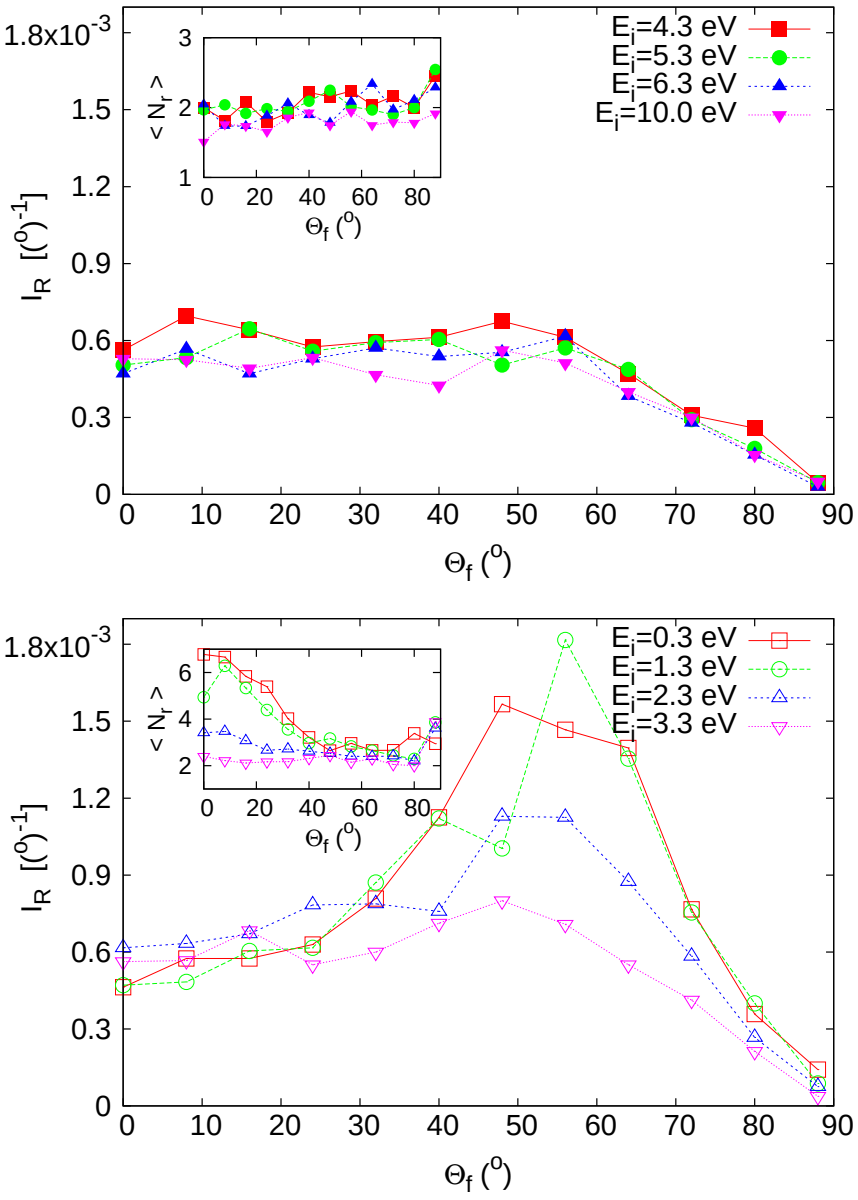

Figure 7: The individual curves shown in Figure 6 for $E_i = 4.3$ (top panel) and 1.3 eV (bottom panel) are split here into the contributions from trajectories at four z_{min} intervals, where z_{min} is the minimum reached height by the N atom upon reflection.

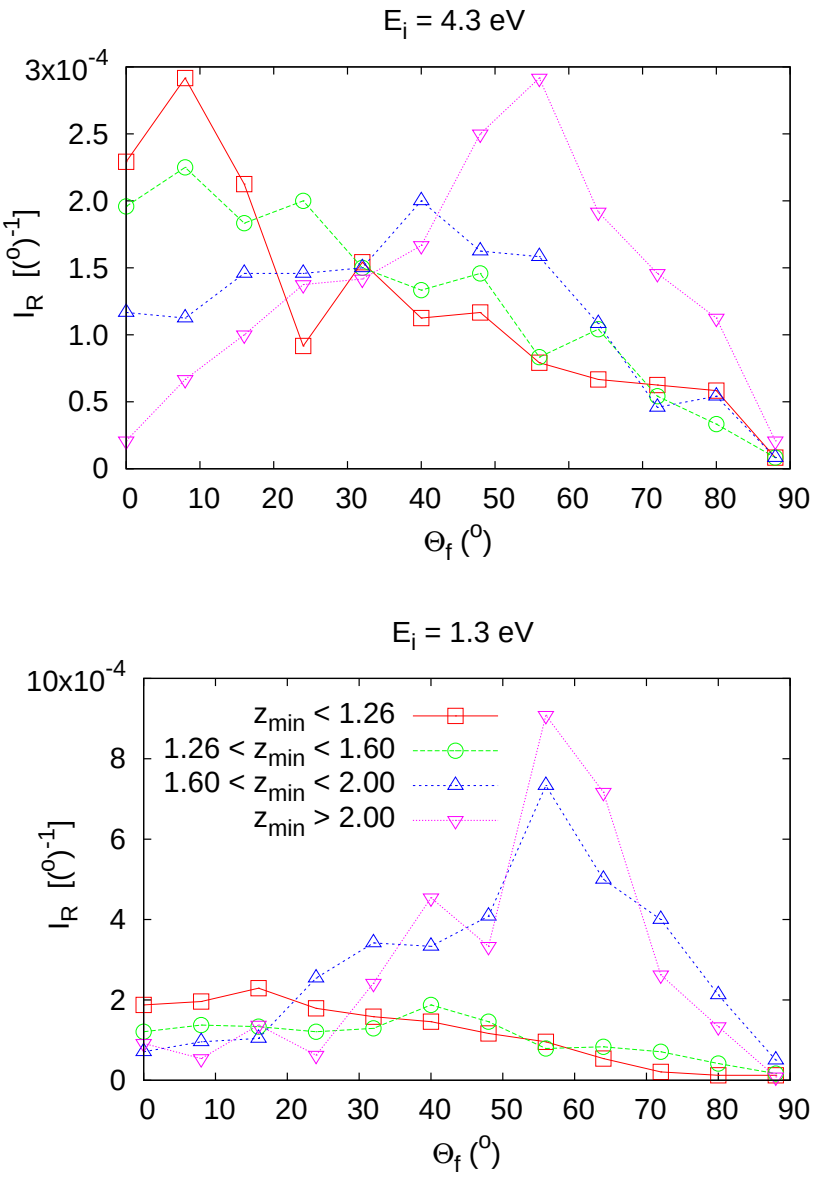

Figure 8: Polar angle distribution of in-plane reflected mono-energetic N atoms using GLO, for individual incident energies E_i. Top and bottom panels show high and low energy regimes, respectively. The inset shows the corresponding average energy lost by the N atoms.

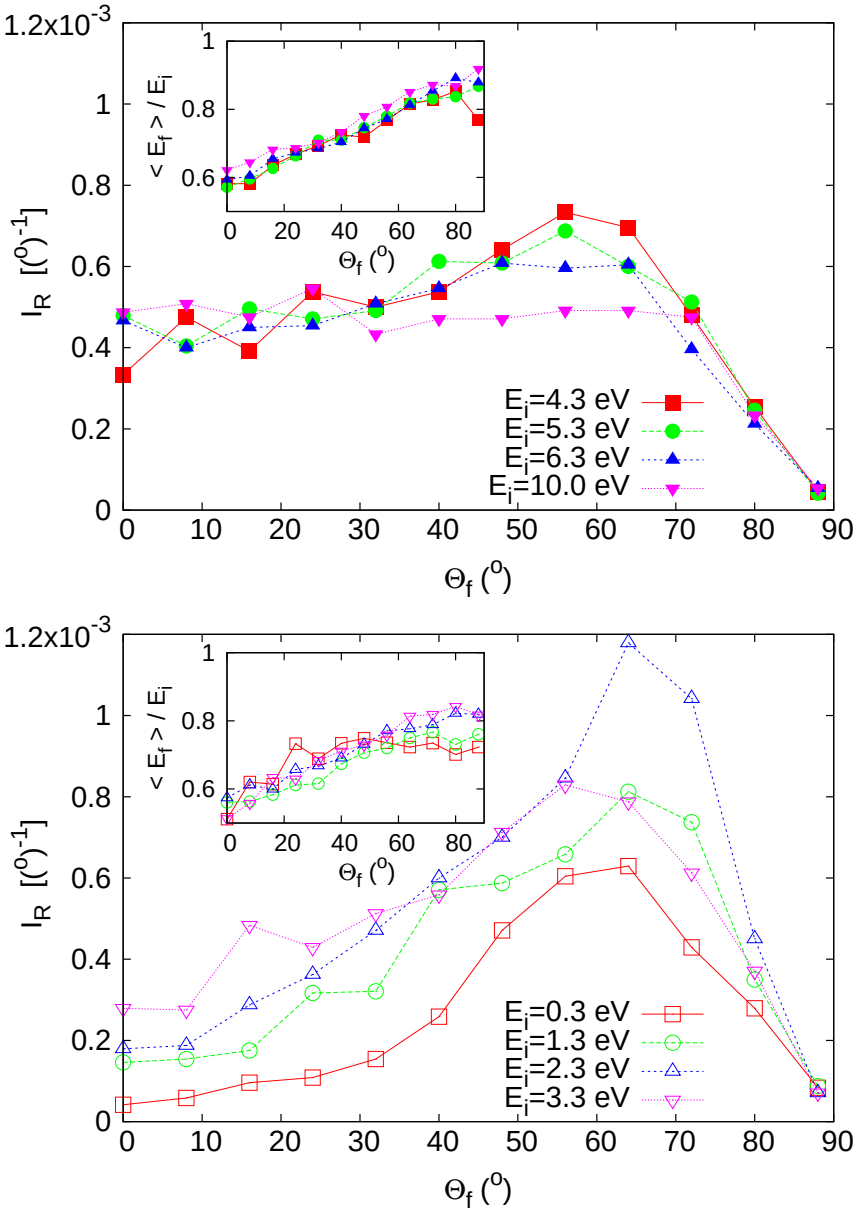

Figure 9: As in Figure 7, the $E_i = 4.3, 1.3$ eV curves from Figure 8 are resolved into contributions from four z_{min} intervals.

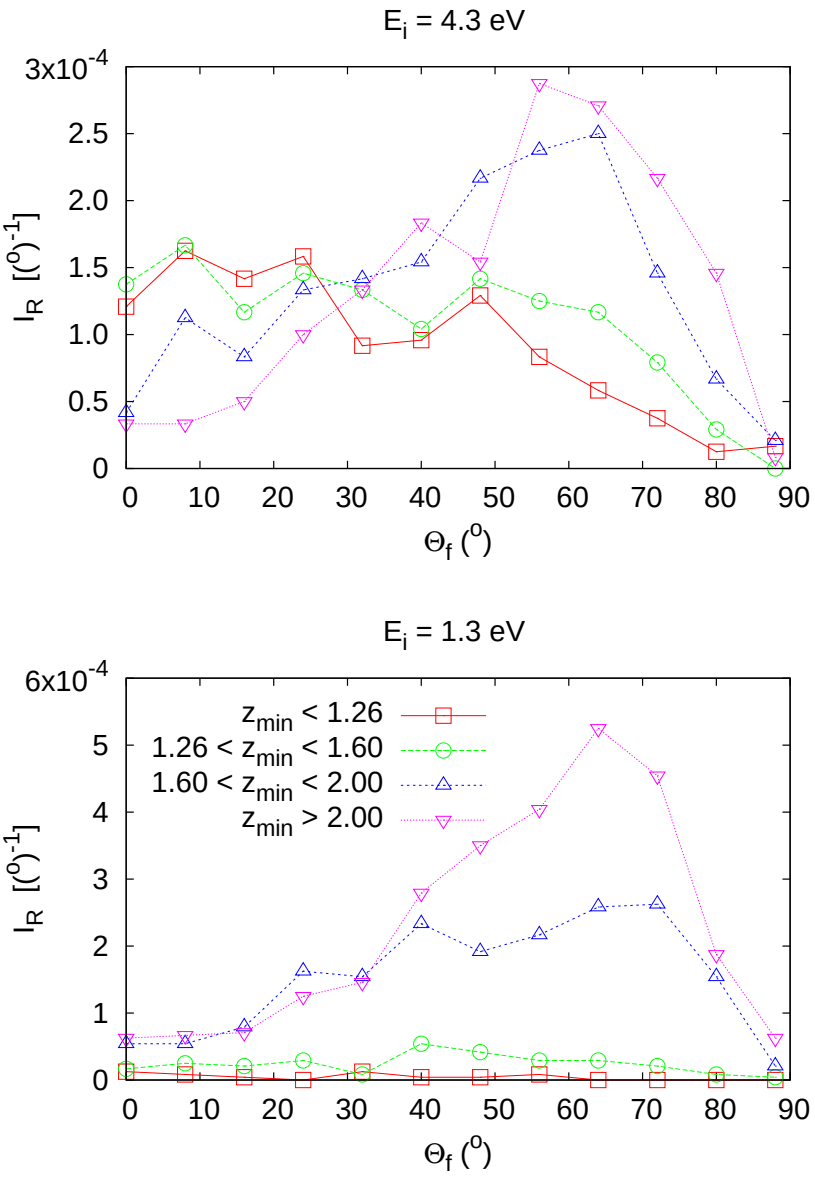

Figure 10: Main graph: sticking probability of N atoms at $\Theta_i = 60^\circ$ as a function of the incident kinetic energy, E_i. This plot accounts for all reflected N atoms, not just the in-plane ones. Top inset: initial (grey) and final (black) (x,y) coordinates in the (1×1) unit cell of the N atoms that possess initial $E_i = 4.3$ eV and end up adsorbed on the surface. Only 5000 trajectories are depicted in this inset. Bottom inset: average number of rebounds undergone by the reflected N atoms using GLO (squares) and adiabatic (circles) dynamics.